Water Resources Research

RESEARCH ARTICLE
10.1029/2020WR027199

Predicting Water and Sediment Partitioning in a Delta Channel Network Under Varying Discharge Conditions

Tian Y. Dong[1], Jeffrey A. Nittrouer[1], Brandon McElroy[2], Elena Il'icheva[3,4], Maksim Pavlov[3], Hongbo Ma[1], Andrew J. Moodie[1], and Vsevolod M. Moreido[5]

[1]Department of Earth, Environmental, and Planetary Sciences, Rice University, Houston, TX, USA, [2]Department of Geology and Geophysics, University of Wyoming, Laramie, WY, USA, [3]Laboratory of Hydrology and Climatology, V.B. Sochava Institute of Geography, Siberian Branch Russian Academy of Sciences, Irkutsk, Russia, [4]Department of Hydrology and Environmental Sciences, Irkutsk State University, Irkutsk, Russia, [5]Water Problems Institute, Russian Academy of Sciences, Moscow, Russia

Abstract Channel bifurcations control the distribution of water and sediment in deltas, and the routing of these materials facilitates land building in coastal regions. Yet few practical methods exist to provide accurate predictions of flow partitioning at multiple bifurcations within a distributary channel network. Herein, multiple nodal relations that predict flow partitioning at individual bifurcations, utilizing various hydraulic and channel planform parameters, are tested against field data collected from the Selenga River delta, Russia. The data set includes 2.5 months of time-continuous, synoptic measurements of water and sediment discharge partitioning covering a flood hydrograph. Results show that width, sinuosity, and bifurcation angle are the best remotely sensed, while cross-sectional area and flow depth are the best field measured nodal relation variables to predict flow partitioning. These nodal relations are incorporated into a graph model, thus developing a generalized framework that predicts partitioning of water discharge and total, suspended, and bedload sediment discharge in deltas. Results from the model tested well against field data produced for the Wax Lake, Selenga, and Lena River deltas. When solely using remotely sensed variables, the generalized framework is especially suitable for modeling applications in large-scale delta systems, where data and field accessibility are limited.

Key Points:
- Channel width, sinuosity, and bifurcation angle are the best remotely sensed, nodal relation variables for predicting flow partitioning
- Channel cross-sectional area and flow depth are the best field measured, nodal relation variables for predicting flow partitioning
- A field validated graph model is developed to accurately predict flux distribution in deltas, where gauge data are limited

Supporting Information:
- Supporting Information S1

Correspondence to:
T. Y. Dong,
tian.tyler.dong@gmail.com

Citation:
Dong, T. Y., Nittrouer, J. A., McElroy, B., Il'icheva, E., Pavlov, M., Ma, H., et al. (2020). Predicting water and sediment partitioning in a delta channel network under varying discharge conditions. *Water Resources Research*, *56*, e2020WR027199. https://doi.org/10.1029/2020WR027199

Received 24 JAN 2020
Accepted 28 OCT 2020
Accepted article online 1 NOV 2020

1. Introduction

River deltas typically contain networks of bifurcating channels that distribute water, sediment, nutrients, and carbon from upstream sources to downstream wetlands and coastlines (Syvitski & Saito, 2007). The distribution of materials nourishes coastal-deltaic environments and facilitates diverse ecosystems that support varieties of biota (Vörösmarty et al., 2009). Overtime, accumulation of biogenic and sedimentary materials contributes to the construction of stratigraphy, which records past environmental conditions, such as fluctuating base level. Understanding what controls flow partitioning at bifurcations is particularly relevant today, as deltaic systems are threatened by reduced water and sediment supplies due to damming and artificial levees (Blum & Roberts, 2009; Graf, 2006; Hoitink et al., 2020; Nienhuis et al., 2020; Paola et al., 2011; Syvitski et al., 2009, 2005; Vörösmarty et al., 2009).

Methods to accurately predict water and sediment routing are useful for estimating delta responses to environmental and anthropogenic stresses (Passalacqua, 2017). At individual bifurcation scale, previous research analyzing partitioning of water and sediment have utilized field surveys, and numerical and physical experiments, for various river morphologies, channel bed sediment composition, and boundary condition perturbations (Bolla Pittaluga et al., 2003; Edmonds & Slingerland, 2008; Kleinhans et al., 2008; Redolfi et al., 2019; Salter et al., 2018; Slingerland & Smith, 1998; Szupiany et al., 2012; Wang et al., 1995). In particular, one-dimensional morphodynamic models have been used to evaluate bifurcation stability by coupling downstream branches to an upstream branch at a bifurcation node, with a nodal relation to describe water and sediment partitioning among the two downstream channels (Bolla Pittaluga et al., 2003; Kleinhans et al., 2008; Wang et al., 1995). These studies determined that symmetrical bifurcations are often unstable (Bolla Pittaluga et al., 2015; Edmonds & Slingerland, 2008; Kleinhans et al., 2008, 2011; Miori et al., 2006;

Schielen & Blom, 2018). Thus, most natural and simulated bifurcations possess asymmetrical flow partitioning (i.e., one branch conveys more flow), as supported by Delft3D models, physical experiments, and field observations (Bertoldi & Tubino, 2007; Edmonds & Slingerland, 2008; Kleinhans et al., 2008). However, because deltas generally contain multiple bifurcations, the one-dimensional models lack sufficient spatial coverage to accurately predict flow partitioning in distributary networks.

At larger spatial scales, channel bifurcations join together, forming a distributary network that delivers water and sediment to the shoreline. At this scale, previous research has developed quantitative metrics to characterize the delta network, such as the distributions of island size and nourishment area (Edmonds et al., 2011; Passalacqua et al., 2013). While these metrics are useful for understanding structure of the delta network, they have limited capacity to predict flow partitioning because flow and sediment transport at a given bifurcation are not constrained explicitly. On the other hand, network-scale hydrodynamic simulations are capable of modeling flow partitioning for an entire delta, but obtaining reliable predictions necessitate detailed channel bathymetry data (Edmonds, 2009; Hiatt & Passalacqua, 2017; Liang et al., 2015; Van et al., 2016). Particularly for large deltas, pursuing field measurements to collect such data for multiple bifurcations is timely and costly.

Recent studies have shown the possibility of modeling flow partitioning in a delta network as a directed acyclic graph (Tejedor et al., 2015a, 2015b, 2018). Therein, advantages of the graph model arise from coupling bifurcation-scale flow approximation and channel network-scale connectivity. Specifically, the ratio of downstream channel width is used in a nodal relation to model flow partitioning at individual bifurcations. But field validation of the modeling outcomes is absent. Moreover, the abilities of other channel hydraulic and planform variables, such as flow depth, sinuosity, and nourishment area, to predict flow partitioning remain unexplained (Appendix A; Edmonds et al., 2011; Gleason & Smith, 2014; Shaw et al., 2016; Sylvester et al., 2019). In addition, as these variables can be measured in the field or via remote sensing techniques, categorizing and analyzing nodal relation predictabilities based on data collection methods can be useful for informing model selection. While field data capture local-scale variabilities in fluid flow and sediment transport, remote sensing data offer greater spatial coverage and accessibility.

Herein, the primary objective of this study is to develop a generalized framework to predict water and sediment movement in a delta network, by coupling nodal relations that describe flow partitioning at bifurcations to an existing graph model that describes network-scale connectivity (Tejedor et al., 2015a). To achieve this objective, a set of hydraulic and channel planform variables are selected, based on the physics of open-channel flow and sediment transport at a bifurcation, to develop the nodal relations, which are then tested against field data collected from the Selenga River delta, Russia (Appendix A). These nodal relations predict partitioning of water discharge, as well as suspended, bedload, and total sediment discharge. The field data set includes continuous measurements of water and sediment discharge partitioning at six bifurcations on the delta over a 2.5-month flood hydrograph, as well as remotely sensed measurements of various channel planform parameters, such as sinuosity (Table 1). The nodal relations are categorized into two groups based on collection methods of the variables: Type I is field measured and Type II is remotely sensed. Performance of the Type I and Type II nodal relations is used to assess model applicability for large delta systems, where gauge data and field accessibility are limited. Finally, model predictions are tested against field measurements collected from the Wax Lake, Selenga, and Lena River deltas.

2. Selenga River Delta

The Selenga River delta resides on the southeastern shore of Lake Baikal in southern Siberia, Russia (Figures 1a and 1b). The lake is formed as part of a rifting basin, initiated ~35 million years ago (Krivonogov & Safonova, 2017). The Selenga River is the largest water and sediment source to Lake Baikal. The delta covers ~600 km^2 and contains numerous distributary channels that receive varying amounts of water and sediment (Chalov et al., 2016; Il'icheva, 2008; Pavlov et al., 2019). Previous studies have classified the orders of distributary channels based on the Hack (1957) topological method (Dong et al., 2016, 2019). In particular, the Selenga River mainstem is classified as a first-order channel and the delta system bifurcates downstream into two second-order channels, and so on, with a total of nine identified channel orders (Figure 1c). Within this network, channel geometry, bed and bank material sizes, vegetation type, and bank morphology vary spatially (Dong et al., 2016, 2019; Il'icheva et al., 2015; Pietroń et al., 2018).

Table 1
Nodal Relations for Predicting Water and Sediment Partitioning Tested in This Study

	Nodal relations for Q	Nodal relations for Q_s
Hydraulic variables		
A—cross-sectional area	$Q_b = \frac{A_b}{A_b + A_c} Q_a$	$Q_{s,b} = \frac{A_b}{A_b + A_c} Q_{s,a}$
B—width	$Q_b = \frac{B_b}{B_b + B_c} Q_a$	$Q_{s,b} = \frac{B_b}{B_b + B_c} Q_{s,a}$
H—thalweg depth	$Q_b = \frac{H_b}{H_b + H_c} Q_a$	$Q_{s,b} = \frac{H_b}{H_b + H_c} Q_{s,a}$
S_{ws}—water surface slope	$Q_b = \frac{S_{ws,b}}{S_{ws,b} + S_{ws,c}} Q_a$	$Q_{s,b} = \frac{S_{ws,b}}{S_{ws,b} + S_{ws,c}} Q_{s,a}$
C_z—Chezy coefficient	$Q_b = \frac{C_{z,b}}{Cz,\ b + Cz,\ c} Q_a$	$Q_{s,b} = \frac{Cz,\ b}{Cz,\ b + Cz,\ c} Q_{s,a}$
Q—water discharge	—	$Q_{s,b} = \frac{Q_b}{Q_b + Q_c} Q_{s,a}$
Planform variables[a]		
B—width	$Q_b = \frac{B_b}{B_b + B_c} Q_a$	$Q_{s,b} = \frac{B_b}{B_b + B_c} Q_{s,a}$
L—branch length	$Q_b = \frac{B_b L_c}{B_b L_c + B_c L_b} Q_a$	$Q_{s,b} = \frac{B_b L_c}{B_b L_c + B_c L_b} Q_{s,a}$
Ω—sinuosity	$Q_b = \frac{B_b \Omega_c}{B_b \Omega_c + B_c \Omega_b} Q_a$	$Q_{s,b} = \frac{B_b \Omega_c}{B_b \Omega_c + B_c \Omega_b} Q_{s,a}$
A_n—nourishment area	$Q_b = \frac{B_b A_{n,b}}{B_b A_{n,b} + B_c A_{n,c}} Q_a$	$Q_{s,b} = \frac{B_b A_{n,b}}{B_b A_{n,b} + B_c A_{n,c}} Q_{s,a}$
R_c—radius of curvature	$Q_b = \frac{B_b R_{c,b}}{B_b R_{c,b} + B_c R_{c,c}} Q_a$	$Q_{s,b} = \frac{B_b R_{c,b}}{B_b R_{c,b} + B_c R_{c,c}} Q_{s,a}$
θ—bifurcation angle	$Q_b = \frac{B_b \theta_b}{B_b \theta_b + B_c \theta_c} Q_a$	$Q_{s,b} = \frac{B_b \theta_b}{B_b \theta_b + B_c \theta_c} Q_{s,a}$

[a]Obtained via remote sensing.

Specifically, both median bed and bank sediment grain size fine downstream, over ~35 km of distance, from gravel at the delta apex to very fine sand and silt at the shoreline. This downstream fining is attributed to a reduction in sediment transport capacity as water discharge is partitioned among the bifurcating channel network (Dong et al., 2016). Understanding this flow partitioning on the delta is critical for assessing land growth. As previously documented, flow partitioning on the delta is a function of river water discharge (Il'icheva, 2008; Il'icheva et al., 2015). However, as measurements are spatially limited and not collected time synchronously, this finding is inconclusive.

3. Methods

3.1. Developing and Evaluating Nodal Relations to Predict Flow Partitioning

Nodal relations utilizing different hydraulic and planform variables are tested using data collected from the Selenga River delta (Table 1). These variables are selected based on their impacts on fluid flow and sediment transport at a bifurcation (see Appendix A for detailed rationale). The nodal relations are then categorized into two groups based on the data collection methods: Type I—field measured and Type II—remotely sensed (Table 1). Following the convention of Wang et al. (1995) and Bolla Pittaluga et al. (2003), generalized Type I relation is expressed as follows:

$$Q_b = \frac{x_b}{x_b + x_c} Q_a + \epsilon, \tag{1}$$

where x_b and x_c are hydraulic variables of interest for the downstream branches, such that $x_b = f(A_b, B_b, H_b, S_b, C_{z,b})$, where A is cross-sectional area, H is depth, B is width, S is water surface slope, and C_z is dimensionless Chezy coefficient, Q_a is the upstream water discharge, ϵ is the residual, and b and c denote the subordinate branches (Table 1). Herein, Type I relations have three explanatory variables, including one hydraulic parameter for each of the downstream branches and the upstream discharge.

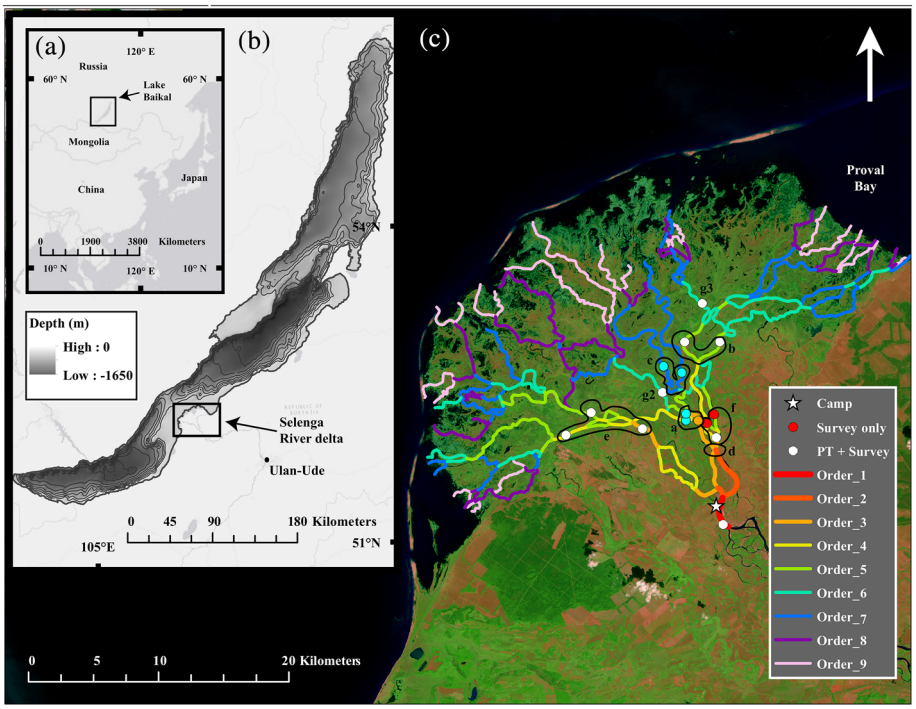

Figure 1. (a) Lake Baikal is located in southeastern Siberia, Russia. (b) Bathymetric map of Lake Baikal, with the location of the Selenga River delta indicated in the black box. (c) Sentinel-2 image of the Selenga River delta showing survey locations from summer 2018. Orange circle indicates survey transect CSELT2, where hydraulic data are provided in the main text. Light blue circles indicate transects in contact with relic fluvial terraces. Black letters mark the six bifurcation locations, where time series measurements of channel geometry, and water and sediment discharge are used for analyzing nodal relations under varying discharge conditions, corresponding to the subplot panels in Figure 8.

Generalized Type II relation is similar to Type I, with the exception that channel width is always included as an additional pair of explanatory variables, shown as:

$$Q_b = \frac{x_{r,b} B_b}{x_{r,b} B_b + x_{r,c} B_c} Q_a + \epsilon, \tag{2}$$

because width is the conventional remotely sensed parameter used to estimate discharge, in addition to being a variable that may also be measured directly in the field (Gleason & Smith, 2014). Here, $x_{r,b}$ and $x_{r,c}$ are remotely sensed channel planform variables of interest for the downstream branches, such that $x_{r,c} = f(L_b, \Omega_b, A_{n,b}, R_{c,b}, \Theta_b)$, where L is channel length, Ω is sinuosity, A_n is nourishment area, R_c is radius of curvature, and Θ_b is bifurcation angle.

These nodal relations are evaluated using standard statistics for linear correlation: coefficient of determination (R^2), normalized root-mean-square error (nRMSE), and Pearson's correlation coefficient (PCC). Moreover, to determine the relative predictabilities of the Type I and Type II relations, Akaike information criterion (AIC) is used (see details in Appendix B; Anderson & Burnham, 2004; Dong et al., 2019). Regression methods that minimize ϵ are not used, as the goal of this study is to evaluate the relative predicative quality among different hydraulic variables on flow partitioning to develop the aforementioned general framework, rather than to optimize the nodal relation for a specific delta system.

3.2. Developing a Generalized Framework to Predict Flux Distribution on Delta Networks

To develop a generalized framework that predicts flux distribution in a delta network, an existing graph model is coupled with the best predictive Type II nodal relations. In particular, steady-state flux in a delta channel network is approximated using a rooted directed acyclic graph with channels as links and bifurcation as nodes (Tejedor et al., 2015a). Link directions correspond to the flow direction in the channels. Each

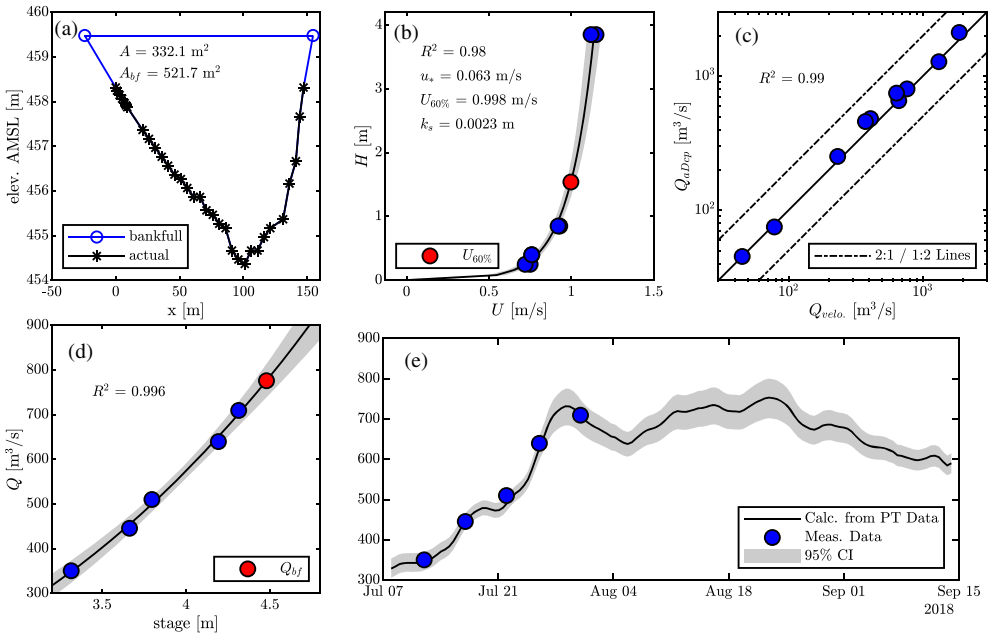

Figure 2. Hydraulic data measured at each survey transect. Shown here are examples collected from transect CSELT2 on July 12th, marked as an orange circle in Figures 1c and 4c and 4d. The data include (a) channel cross-sectional profile, (b) velocity profile, (c) comparison between calculated water discharge (Q) using velocimeter data and measured water discharge using an aDcp, at 10 survey transects, (d) rating-curve model of Q, and (e) hydrograph for the entire survey duration.

link contains hydraulic information such as channel width and sinuosity, which are used in the nodal relations to predict water and sediment flux distribution for the entire network (Tejedor et al., 2015a). Since Type II nodal relations for water and sediment partitioning contain variables that are measured solely by remote sensing techniques, the modified graph model can be used to predict flux distribution in deltas worldwide with minimum field information.

3.3. Field Data Collection

Point measurements of flow velocity and water samples (to measure suspended sediment concentration), channel geometry, bedload transport rates, and stage were collected from the Selenga River delta at 16 transects during a 6-week field campaign over summer 2018 (Figure 1c). Transect locations were strategically selected to constrain flow partitioning across the bifurcating delta network. Specifically, water and sediment fluxes at the chosen locations control nourishment to the entire deltaic shoreline. In addition, they are located within the seven main distributary channels of the delta, which convey more than 75% of the main river flow (Il'icheva, 2008; Il'icheva et al., 2015). Moreover, the transects were located in single-thread and straight reaches within normal flow region of the delta, so as to reduce the effects of local perturbations on hydraulics. At each transect, point measurements of velocity were collected from the thalweg using a mechanical velocimeter. A bottle sampler was used to collect water samples, from which sediment concentration was subsequently measured. Specifically, four-point measurements of velocity and sediment concentration were collected at 10, 15, and 45 cm above the channel bed and at the water surface (Figure 2b; typically corresponding to ~5%, ~10%, ~25%, and 100% of the flow depth, respectively). A bedload sampler with a width and height of 50 and 15 cm, respectively, was deployed in the thalweg for 2–5 min to measure bedload transport rates (Emmett, 1979). Channel cross-sectional dimensions (width and depth) were measured using a LOWRANCE single-beam sonar (Figure 2a). Stage was measured using an ONSET HOBO pressure transducer at each transect. Absolute elevations of the pressure transducers were measured using a JAVAD differential Global Navigation Satellite System (GNSS). Each transect was visited once every 5–6 days, thus totaling five visits at each transect for the duration of the field campaign (6 weeks). The data were used to establish sediment and water discharge rating curves.

3.3.1. Measuring Water and Sediment Discharge

Assuming hydraulically rough flow, a law-of-the-wall model is fit to the measured velocity profiles via ordinary least square method (Garcia, 2008). Flow velocity at 60% depth below the water surface ($U_{60\%}$, shown as the red circle in Figure 2b) is obtained from the model and used to calculate water discharge, such that $Q_{velo.} = U_{60\%}A$, where A is cross-sectional area (Figure 2b; Rantz et al., 1982). To validate the calculated water discharge, a selection of $Q_{velo.}$ is compared to water discharge (Q_{aDcp}) measured by an acoustic Doppler current profiler (aDcp) at 10 different survey transects. Water discharge measured by the aDcp confirms calculated water discharge using velocity data (Figure 2c).

Sediment samples were processed at the V.B. Sochava Institute of Geography in Irkutsk, Russia. Water samples were filtered using 3-μm ash-free paper filters. Organic matter was removed from the filters following a standard loss on ignition method, with the sample reweighed to obtain inorganic mass; this value was subsequently converted to volume assuming a sediment density of 2,650 kg/m^3 (Heiri et al., 2001). A depth-averaged sediment concentration is multiplied by water discharge to obtain suspended sediment discharge. Bedload samples were air dried and weighed. Bedload transport rates, measured as mass per-unit-time, were converted to volumetric bedload flux per-unit-channel width after accounting for sediment density and sampler width (50 cm). Bedload discharge is calculated by multiplying measured flux and channel width. Total sediment discharge (Q_s) equals the sum of suspended and bedload sediment discharge at each survey transect.

3.3.2. Building Both Rating-Curve Models and Flood Hydrographs

Water and sediment rating-curve models at each transect are developed by fitting measured stage, and water and sediment discharge, using nonlinear least squares method (fitnlm in MATLAB; Figure 2d), such that $Q_i = \alpha G_i^{\beta} + \epsilon$, where i denotes the ith transect and G is stage, which is obtained by subtracting average lake surface elevation (455 m above mean sea level; Il'icheva et al., 2015) from the measured water surface elevation at each transect (Rantz et al., 1982). α and β are transect-specific rating curve constants, and ϵ is uncertainty.

A hydrograph for each transect is obtained by combining the rating-curve model with time series stage data (~72 days). Stage data are recorded as absolute pressure (p) by the pressure transducers. Water height (z) above the pressure transducer is calculated via $z = (p - p_{atm})/\rho g$, where p_{atm} is atmospheric pressure, ρ is density of water, and g is gravitational acceleration. A time series of water surface elevation is constrained by adding z to absolute elevations of the pressure transducers surveyed by the JAVAD GNSS. The data are then smoothed over a 12-hr window to reduce fine-scale water elevation changes due to wind and/or local hydraulic conditions (i.e., smoothdata in MATLAB). The resulting water elevation data are converted to stage by subtracting the average lake surface elevation. Finally, a 2.5-month-long hydrograph model is obtained by combining a time series of stage data with the rating-curve model at each of the 16 transects (Figure 2e). Bankfull discharge for each transect is calculated using the rating-curve model with the assumption that bankfull stage equals the elevation of the bank top. As channels at a few transects are eroding into Quaternary-aged fluvial terraces, bank elevations may not be built by modern floodplain depositional processes (highlighted by light blue circles in Figure 1c; Dong et al., 2019). Bankfull stages at these transects are modified by 0.5 m, as it has been documented that stage at effective discharge conditions is ~0.5–1 m below these terraces (Gyninova & Korsunov, 2006). There are two survey transects that did not have time series stage data due to instrumentation failure (marked by red circles in Figures 1c and 4c and 4d). However, all other hydraulic measurements were recorded. Finally, a time series of sediment discharge for each transect is produced using the same method as the hydrograph and combining a sediment rating curve with time series stage data.

3.3.3. Measuring Planform and Additional Hydraulic Variables

Nourishment area in the Selenga River delta is identified using the aforementioned graph model (section 3.2 and Appendix A; Tejedor et al., 2015a). Determining the true nourishment area necessitates constraints on flow direction and connectivity of the floodplain (Edmonds et al., 2011; Shaw et al., 2016). Due to an absence of such a data set, nourishment area boundaries are set as a distance of one channel width, extending perpendicular from the bankline, rather than making assumptions about floodplain connectivity. This approach thus produces a minimum (conservative) nourishment area for each node.

All planform variables are extracted from a Sentinel-2 image from June 2017 (Appendix A and Figure 1c). Channel sinuosity (Ω) and length (L) are measured for each channel reach, which is the stretch of

Table 2
Performance of Various Nodal Relations for Estimating Water and Sediment Partitioning

	Nodal relations for Q					Nodal relations for Q_s				
	R^2	PCC	nRMSE	AIC	Δ AIC[a]	R^2	PCC	nRMSE	AIC	Δ AIC[a]
Hydraulic variables										
A—cross-sectional area	0.98	0.99	0.08	557.6[b]	—	0.83	0.91	0.49	−451.9	4.4
H—thalweg depth	0.95	0.97	0.14	622.4	64.8	0.77	0.88	0.57	−434.0	22.3
B—width	0.88	0.94	0.20	668.7	111.1	0.74	0.86	0.60	−428.5	27.8
C_z—Chezy coefficient	0.87	0.94	0.21	675.9	118.3	0.59	0.77	0.75	−400.7	55.6
S_{ws}—water surface slope	0.60	0.81	0.37	742.3	184.7	0.70	0.84	0.65	−418.7	37.6
Q—water discharge	—	—	—	—	—	0.84	0.92	0.47	−456.3[b]	—
Planform variables[c]										
Ω—sinuosity	0.90	0.95	0.19	663.4	105.8	0.79	0.89	0.54	−436.0	20.3
A_n—nourishment area	0.52	0.78	0.41	757.8	200.2	0.40	0.67	0.91	−373.6	82.7
L—branch length	0.46	0.82	0.43	764.6	207.0	0.77	0.88	0.56	−431.3	25.0
θ—bifurcation angle	0.45	0.79	0.44	766.7	209.1	0.77	0.88	0.57	−430.2	26.1
R_c—radius of curvature	0.43	0.77	0.44	768.0	210.4	0.71	0.85	0.63	−417.6	38.7

[a]$\Delta AIC = AIC - AIC_{min}$. [b]$AIC_{min}$. [c]Remotely sensed.

channel bounded by bifurcation nodes at both upstream and downstream ends. Radius of curvature (R_c) and the bifurcation angle (Θ) are measured following the method of Fagherazzi et al. (2004) and Coffey and Shaw (2017), respectively (Figure A1).

Another two hydraulic variables used for the nodal relation models are dimensionless Chezy coefficient (C_z) and water surface slope (S_{ws}). Chezy coefficient is defined as $C_z = U/u_*$ (Garcia, 2008), where u_* is shear velocity and U is depth-averaged flow velocity calculated from the measured velocity profiles (Figure 2b). Water surface slope at each transect is calculated using the difference in water surface elevation between the transect of interest and its nearest upstream or downstream neighbor, such that $S_{ws} = \Delta h/\Delta x$, where h is the water surface elevation. Streamwise distance (Δx) between two adjacent transects ranges 1.2–7.3 km. Therefore, this value represents a reach average slope rather than the local slope at the bifurcation node.

4. Results

4.1. Nodal Relations for Water and Sediment Partitioning

Twenty-one nodal relations are developed and evaluated based on their predictive qualities, given field data of flow partitioning, measured at six bifurcations on the Selenga River delta (Tables 1 and 2, Figure 3, and supporting information). These models are categorized into two groups based on the data collection methods: Type I models—field measured and Type II models—remotely sensed (Table 1). Variables used by Type I models include cross-sectional area (A), channel width (B), thalweg depth (H), water surface slope (S_{ws}), and dimensionless Chezy coefficient (C_z). Variables used by Type II models include channel width (B), length (L), sinuosity (Ω), nourishment area (A_n), radius of curvature (R_c), and bifurcation angle (Θ). All models share a common explanatory variable: water and sediment discharge in the upstream branch (Q_a).

Each model type predicts total, suspended, and bedload sediment and water discharge in the downstream branches. Variables of each model type are evaluated based on the amount of variance explained in the measured flow in the downstream branches (i.e., Q_b and Q_c) using R^2, PCC, and nRMSE as metrics. Furthermore, variables are ranked in a descending order based on their predictability (i.e., variable with largest R^2 or smallest nRMSE is ranked first). For clarity, the most predictive Type I and II models for each discharge type are shown in the main text, and results of other model evaluations are shown in the supporting information (Figure 3).

For partitioning of water discharge, a Type I model utilizing cross-sectional area (A) ratio of the downstream branches has the greatest predictive quality (Figure 3a and Table 2). Other Type I model variables are ranked by their relative predictive qualities in a descending order: H, B, C_z, and S_{ws} (Table 2). For Type II models, a nodal relation that uses B and Ω ratios of the downstream branches has the greatest predictive quality

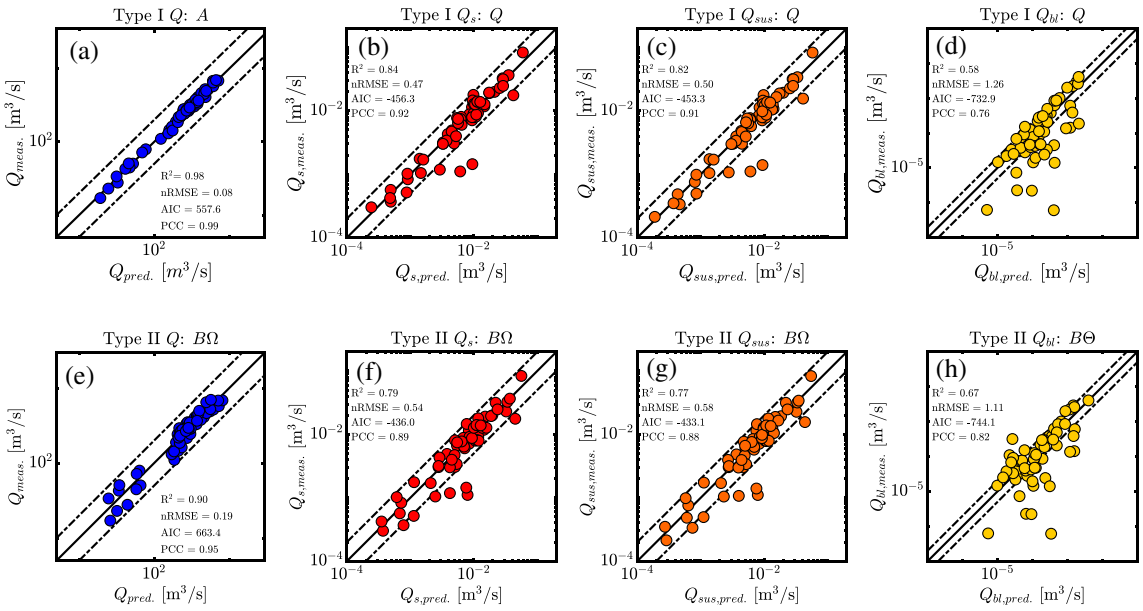

Figure 3. Nodal relation predicted versus field measured total, suspended, and bedload sediment and water discharge using different hydraulic and channel planform variables (Tables 1 and 2). The dashed lines are 1:2 and 2:1 lines. Type I models are shown in panels (a)–(d), and Type II models are shown in panels (e)–(h).

(Figure 3e and Table 2). Other Type II model variables are ranked by their relative predictive qualities in a descending order: B with L, A_n, Θ, and R_c (Table 2).

For partitioning of total, suspended, and bedload sediment discharge, a Type I model that uses the measured water discharge (Q) ratio of the downstream branches has the greatest predictive quality (Figures 3b–3d and Table 2). The other Type I model variables, ranked in a descending order in terms of their relative predictive qualities, are A, H, B, S_{ws}, and C_z (Table 2). For Type II models, a nodal relation that utilizes B and Ω has the best predictive quality for total and suspended sediment discharge, followed by B with L, Θ, A_n, and R_c, in a descending order of relative predictive qualities (Figures 3f and 3g and Table 2; see the supporting information for details). For bedload sediment discharge, a Type II model that uses B and Θ ratio of the downstream branches has the greatest predictive quality (Figure 3h).

4.2. Graph Model Predictions

To develop a generalized framework that predicts flux distribution in a delta network based solely on remotely sensed data, a graph model is coupled with the best predictive Type II nodal relations to predict total, suspended, and bedload sediment and water discharge partitioning (Figure 3). In this graph model, the channel network of the Selenga Delta is characterized by a total of 142 nodes and 183 links (Figures 1c and 4a; Tejedor et al., 2015a). Thirty-two nodes are classified as outlets and are connected directly to Lake Baikal or to the surrounding embayments. Nourishment area for each bifurcation node is also identified, which includes the downstream nodes, links, and outlets that the bifurcation nourishes (Figure 4b). Inputs for this framework are planform variables, including channel width, bifurcation angle, and sinuosity, as well as time series of water or sediment discharge at the delta apex (Figure 1c). Flow partitioning (i.e., $x_{r,b}/(x_{r,b}+x_{r,c})$), Equation 2 in the Type II nodal relations, is assumed to be at steady state (i.e., variables are measured under moderate discharge conditions; Figure 1c Tejedor et al., 2015a). Using input values measured on the Selenga River delta, this method predicts water and sediment discharge at every link of the channel network (Figure 4c). Herein, predicted discharge is normalized by input flow at the main river to yield a relative flux (F), such that $F = Q_i/Q_{main}$. The predicted flux distribution map indicates that major directions of suspended sediment and water transports are toward the eastern and western portions of the delta (Figure 4c). Bedload transport has a similar overall spatial trend, but the western part of the delta receives greater flux compared to the eastern part (Figure 4d).

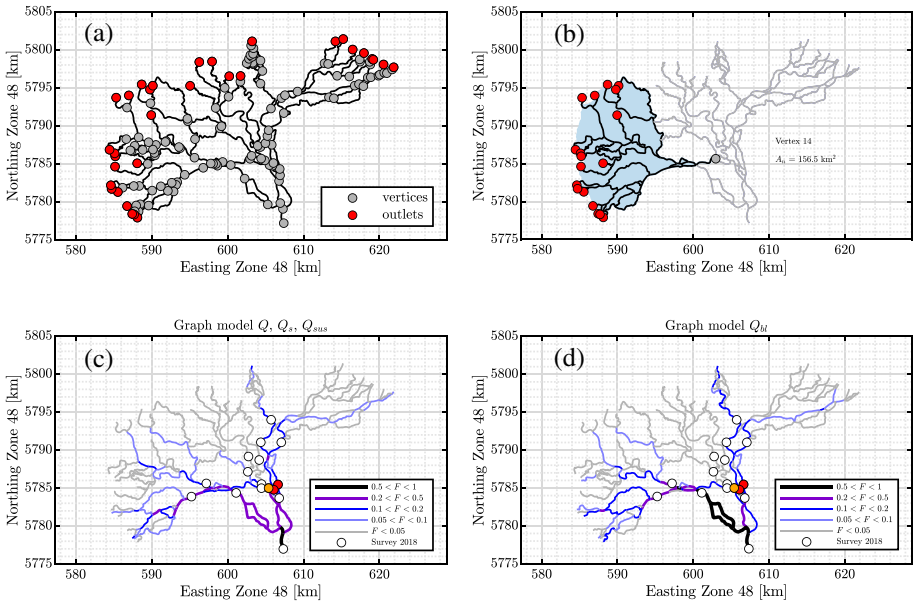

Figure 4. (a) Channel network and nodes of the Selenga River delta. Red circles indicate outlet nodes. (b) An example of nourishment area identified for a bifurcation node (vertex 14). Maps showing graph model predicted (c) total and suspended sediment, and water discharge and (d) bedload discharge distribution over the Selenga River delta. F is the relative flux, a parameter that represents flow in each link as a proportion of the main river flow, such that $F = Q_i/Q_{main}$.

4.3. Field Validation and Model Application

4.3.1. Comparing Measured and Modeled Flux Distributions Over the Selenga Delta

To validate results of the graph model, field measured flux distribution over the Selenga River delta is evaluated based on data collected at the 16 survey transects. Based on connectivity between the branches, flow at 12 additional channel reaches is calculated via mass balance. These 28 channel reaches cover the seven main distributary channels in the Selenga River delta and convey over 75% of the main river flow (Dong et al., 2016; Il'icheva, 2008; Il'icheva et al., 2015). Water discharge at each of the 28 reaches is normalized by the main river, that is, $F = Q_i/Q_{main}$. Values of F are categorized into two groups based on low and flood discharge conditions, separated using a cutoff discharge of $Q = 1{,}350$ m^3/s, a value that is based on flow frequency analysis of historical discharge data (Pietroń et al., 2018). Mean values of F from each group are used to generate maps of measured flux distribution at low and flood discharge conditions (Figure 5).

F is then calculated for the western, middle, and eastern portions of the delta based on a definition proposed by Il'icheva (2008, Figure 5). The results indicate that the Selenga River delta has a diverse pattern of flow partitioning at low discharge: 51.4% of the main river discharge is allocated to the western portion of the delta, 21.8% to the middle region, and 25.5% to the eastern portion at low discharge conditions (Figure 5a and Table 3). At flood discharge, the western, middle, and eastern portions of the delta receiving 49.5%, 25.0%, and 23.4% of the main river discharge, respectively. Differences in flux distribution between low and flood discharge are calculated for each transect, as well as for the branches that are connecting these transects, such that $\%\text{Change} = ((F_{low} - F_{flood})/F_{low}) * 100\%$. %Change increases as a function of distributary channel order, indicating that smaller bifurcations experience a higher-magnitude variability in flow partitioning as stage varies between low and flood discharge (Figure 5c).

Graph model predicted and field measured flux distribution maps qualitatively agree, as a majority of the flow is directed toward the eastern and western portions of the delta (Figures 4c and 5). Quantitatively, field measured and graph model predicted water discharge, and total and suspended sediment discharge, are in agreement (i.e., explaining 94%, 46%, and 43% variance in the field data, respectively; $n = 84$; Figures 6a–6c). This is the first time that the graph model framework has been applied and validated to predict flux distribution. In contrast, bedload sediment discharge is poorly predicted by the graph model (i.e., explaining only 2% of the variance; Figure 6d). Meanwhile, rating curve predicted total and suspended sediment, and water discharge, are also in agreement with field measurements (i.e., explaining 99%,

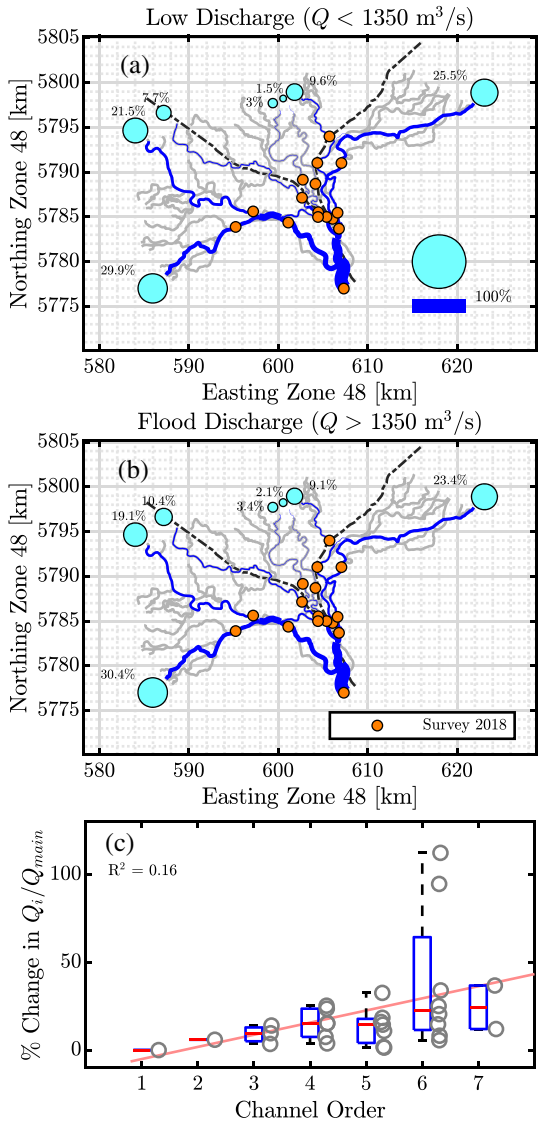

Figure 5. Field measured flux distribution (same as $F = Q_i/Q_{main}$ in Figure 4; see text for details) for the seven main distributary channels of the Selenga River delta at (a) low and (b) flood discharge conditions. Black dashed lines are boundaries proposed by Il'icheva (2008) that divide the delta into western, middle, and eastern portions. The cyan circles and percentage values represent the proportion of flow in the main stem that each of the seven main distributary channels receive at their upstream-most locations, prior to higher-order channel bifurcations (Orders 5–9). (c) Percentage of change in relative flux (F) between low and flood discharge conditions as a function of distributary channel order.

67%, and 65% of the variances respectively; Figures 6e–6g). Moreover, rating curve predicted bedload sediment discharge has the best performance among all sediment discharge types (i.e., explaining 72% of the variance; Figure 6h). Furthermore, the graph model also predicts hydrograph and sediment discharge for each of the 183 channel branches using input time series of water and sediment discharge at the main river and are in agreement with the rating curve predictions within 95% confidence interval (see the supporting information for details).

4.3.2. Measured Flow Partitioning at Bifurcations of the Selenga Delta

Flood peaks arrive nearly simultaneously at all transects on the Selenga River delta, indicating that stage adjustments to varying water discharge are practically instantaneous at the network scale (see Appendix C for cross correlation between hydrographs measured at the main river and at each transect). A rising and a falling limb, and an intermediate stall period, are identified from the main river (delta apex) hydrograph (i.e., findpeaks in MATLAB; Figure 7). To investigate the variability of flow partitioning, rating curve predicted flows at five bifurcations (note: the sixth bifurcation *f* is omitted due to instrumentation failure of the pressure transducers) in the Selenga River delta are depicted as Q_i/Q_a, where Q_a is water discharge from the upstream branch (i.e., $Q_a = Q_b + Q_c$), Q_i is water discharge in one of the downstream branches, and i is an index denoting branch b or c (Figure 8; Salter et al., 2018). Based on mass balance (Equation A1), the sum of Q_i/Q_a must equal 1, and a value of 0.5 indicates equal partitioning between the subordinate branches. Results show that flow partitioning is asymmetrical for all five bifurcations during the rising and falling limbs of the hydrograph. Asymmetry decreases as stage rises in three out of the five bifurcations (Figures 8a–8c). Asymmetry grows for one bifurcation during flood (Figures 8e). Lastly, one bifurcation has quasi-symmetrical flow partitioning during flood condition. The rating curve predicted flow partitioning varies among the five bifurcations during the survey period and is in agreement with field measurements during rising limb of the hydrograph.

To quantify this variability, a range and coefficient of variation (cv) in flow partitioning are calculated at each bifurcation. Ranges of flow partitioning span between 5.3% and 14.7% of water discharge in the upstream branch (Figure 8). cv values of flow partitioning range between 1.8% and 12.1% (Figure 8). Flow partitioning of the graph model is assumed to be steady; therefore, it does not predict the observed variability in short time periods of unsteady adjustment. However, graph model predicted steady-state values are in agreement with the mean rating curve predictions during the stall period and falling limb of the hydrograph, explaining more than 85% of the variance in observed values (Figure 8f). For the rising limb of the hydrograph, agreement between the graph model and rating curve predictions is slightly weaker (Figure 8f).

In practice, each survey at the same transect records a slightly different hydraulic geometry due to minor navigation errors (~10 m), which affects water discharge calculation, and the resulting flow partitioning estimation (Figure 8g). To constrain these errors, upper and lower bounds of flow partitioning are calculated using a range of measured cross-sectional areas ($n = 5$; Figure 8g). Results show that the effects of changing hydraulic geometry on flow partitioning due to navigation errors are negligible (Figure 8).

4.3.3. Application of the Graph Model to Predict Flux Distribution in Other Deltas

The availability of new methods for extracting channel networks and geometry from remotely sensed images has increased drastically over the past 5 years (Hiatt et al., 2019; Isikdogan et al., 2017a, 2017b; Schwenk

Table 3
Hydraulic Variables for Different Portion of the Selenga River Delta

Hydraulic variables	Western portion	Middle portion	Eastern portion
$\bar{S}$	2.53×10^{-4}	1.95×10^{-4}	1.86×10^{-4}
$\bar{A}$ (m^2)	425	115	311
$\bar{H}$ (m)	3.76	2.38	3.85
F_{low}	51.4%	21.8%	25.5%
F_{flood}	49.5%	25.0%	23.4%

et al., 2019). This offers the ability to monitor and measure morphological changes in rivers and deltas, which is especially useful for sites that are not particularly accessible (e.g., the Arctic region). Based on the analysis presented herein, nodal relations utilizing channel width, sinuosity, and bifurcation angle are incorporated into an existing graph model that provides good agreement between measured and predicted flux distribution on the Selenga River delta (Figure 6). This framework is applied to other deltas, to test its applicability where field data exist for additional validation; specifically, the Wax Lake and the Lena River deltas. These data include repeated point measurements of water discharge (Fedorova et al., 2015; Hiatt, 2013; Magritsky et al., 2018) and extensive remotely sensed parameters, such as the channel network, known flow direction, and width measurements (Figure 9; Piliouras & Rowland, 2019; Schwenk et al., 2019; Tejedor et al., 2015a).

A total of 3,253 nodes and 4,596 links is identified for the Lena River delta. One hundred ninety-eight nodes are classified as outlets. The graph model prediction indicates that the majority of water flow is directed toward the western and eastern parts of the delta (Figure 9b). Water discharge from low to flood conditions, measured at nine gauging stations in the delta, are compared to graph model prediction and are in agreement (Figure 9d).

For the Wax Lake delta, a total of 66 nodes and 73 links is identified. Twenty-five nodes are classified as outlets. The graph model prediction indicates that water flow is relatively well distributed among the outlets (Figure 9a). Point measurements of water discharge, collected at 47 survey sites in the delta during moderate discharge condition, are compared to the graph model predictions and are in agreement (Figure 9c; explaining 73% of the variance in measured values Hiatt, 2013).

5. Discussion

5.1. Predictability of the Nodal Relations

Based on the analysis conducted in this study, Type I nodal relations provide accurate predictions of total and suspended sediment, and water discharge partitioning (i.e., explain more than 82% of the variances; Figure 3). Meanwhile, a Type II nodal relation, using width and bifurcation angle, provides accurate predic-

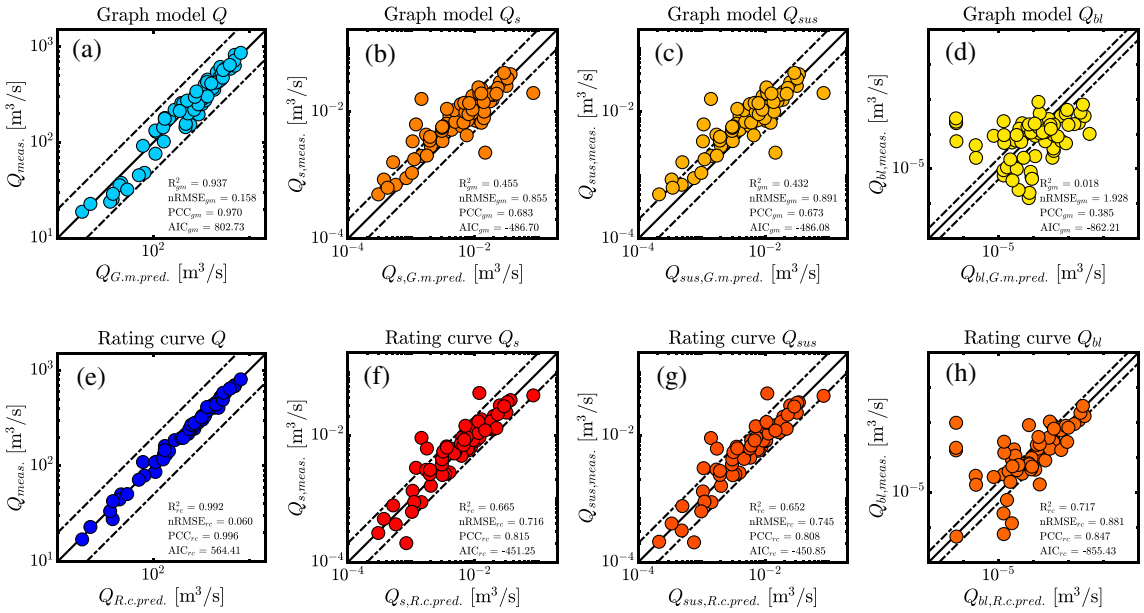

Figure 6. Graph model predicted versus field measured (a) water, (b) total sediment, (c) suspended sediment, and (d) bedload sediment discharge for all transects in the Selenga River delta. Rating curve predicted versus field measured (e) water, (f) total sediment, (g) suspended sediment, and (h) bedload sediment discharge for all transects in the Selenga River delta. The dashed lines are 1:2 and 2:1 lines.

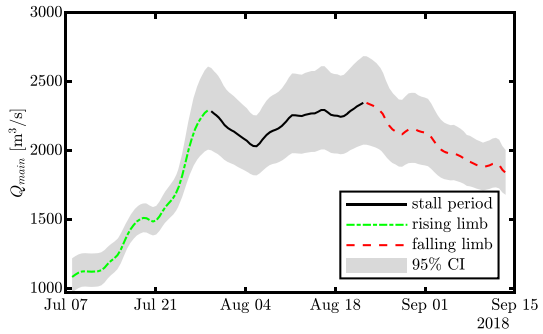

Figure 7. Main river (delta apex) hydrograph is categorized into three sections, a rising and a falling limb, and an intermediate stall period.

tion of bedload discharge partitioning (i.e., explain 67% of the variance; see the supporting information for details). However, despite the model types, prediction of bedload sediment discharge is slightly weaker than other discharge types (Figure 3). Sediment motion on the river bed is highly stochastic and is affected by many factors, including local bed topography, grain hiding effect, and vegetation (Garcia, 2008). Therefore, collecting bedload discharge partitioning data in the field is still the best option for accurate assessment of flux. On the other hand, channel geometry is sufficient for reliable predictions of suspended sediment and water discharge, and thus, in the absence of direct measurements, channel geometry is worthwhile to collect (i.e., explaining 88%, 95%, and 98% variance in measured water discharge using width, depth, and cross-sectional area as predictors; see the supporting information for details). Such a finding is intuitive: as is shown by previous studies on equilibrium hydraulic geometry, rivers adjust their channel dimension to accommodate the upstream input of water and sediment discharge (Dong et al., 2019; Dunne & Jerolmack, 2020; Leopold & Maddock, 1953; Parker, 1978a, 1978b).

In the case where all field data are absent, Type II models are good alternative methods to constrain flow partitioning for river and delta bifurcations. Specifically, despite the simplicity of the Type II models and a lack of calibration, predictions of these nodal relations have similar or better accuracy as the Type I models, explaining only 5–8% less variance (Figure 3). For example, while width is remotely measurable, and a strong predictor of water discharge, analysis herein shows that the combination of width, sinuosity, and bifurcation angle provides better predictions of flow partitioning for all discharge types, including total, suspended, and bedload sediment, and water discharge (Figure 3 and the supporting information). However, it

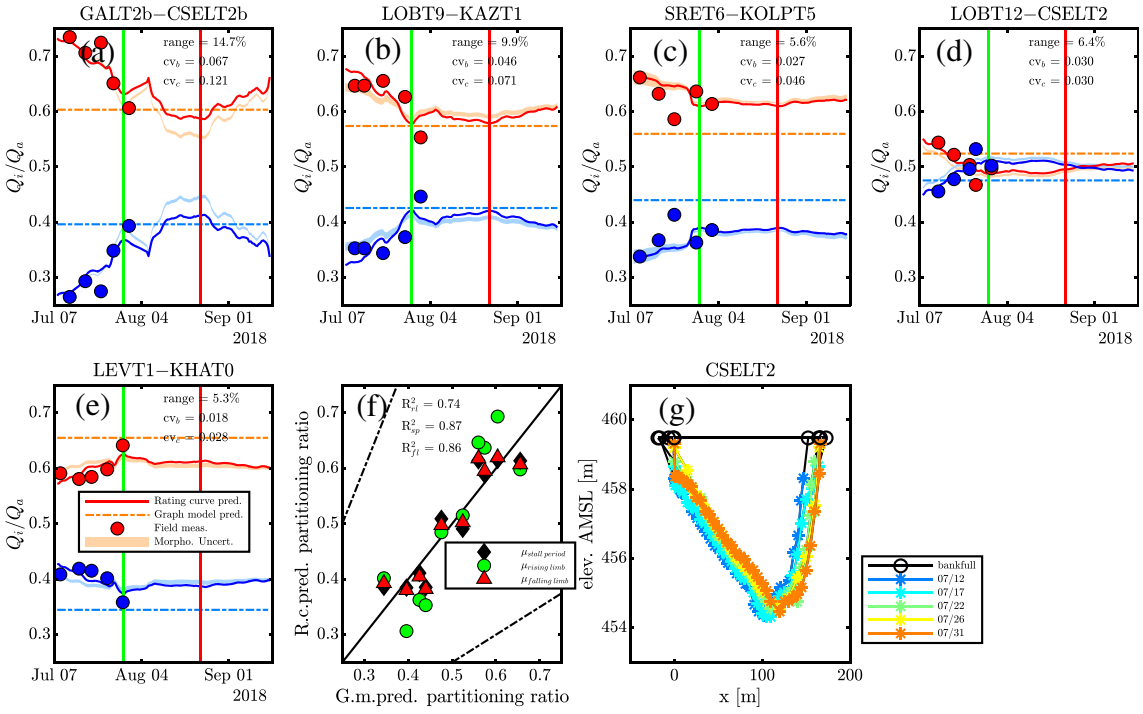

Figure 8. (a–e) Time series of flow partitioning for five bifurcations on the Selenga River delta. Locations of the bifurcations are marked by the black outlines in Figure 1c and labeled with the same letters as the subplot panels. The green and red vertical lines indicate termination of the rising limb and onset of the falling limb of the hydrograph shown in Figure 7. Shaded regions are uncertainties in flow partitioning due to potential error in hydraulic geometry measurements. For this study, Q_b is designated as the downstream branch that conveys a larger proportion of the upstream flow and is indicated by the warm colored lines, while Q_c is indicated by cool colored lines. (f) Rating curve and graph model predicted flow partitioning during rising and falling limb, and stall period of the hydrogrpah. The black dashed lines are 1:2 and 2:1 lines. (g) Cross-section channel profiles measured at transect CSELT2, marked as an orange circle in Figures 1c and 4c and 4d. Differences among the profiles are due to navigation errors.

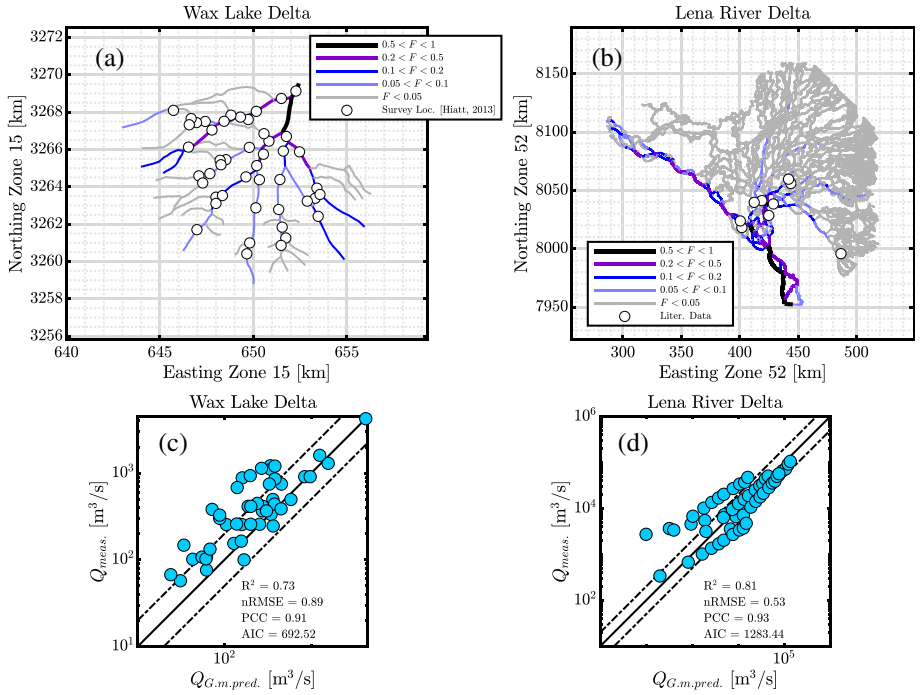

Figure 9. Maps showing graph model predicted water discharge partitioning for (a) Wax Lake delta, USA, and (b) Lena River delta, Russia. (c and d) Graph model predicted versus field measured water discharge for the Wax Lake and Lena River deltas.

is not necessary to use more than two variables, for example, the full Chezy formulation, to predict flow partitioning (Equation A2), because adding explanatory variables with weak predictability does not improve goodness of the fit (e.g., higher R^2 values) but rather increases the amount of data needed to make a better prediction (i.e., decreasing model quality, as shown by the AIC values). For example, as cross-sectional area explains 99% of the variance in the downstream water discharge, adding more variables will not improve model performance (Figure 3a).

5.2. Predictability of the Graph Model

Analysis in this study shows that rating curve models provide the most accurate predictions of water and sediment discharge partitioning. However, collecting a sufficient amount of field data to build reliable rating curves is costly in terms of labor, time, and instrumentation. As a result, rating curve models are often limited spatially, especially for distributary systems, which may contain tens to hundreds of branches. For most delta systems, flow partitioning in the distributary network is unconstrained, because the downstream most gauging station is typically tens to hundreds of kilometers upstream of the apex (Nienhuis et al., 2020). The graph model specifically addresses this problem by only requiring field measured water and sediment discharge at the delta apex (i.e., the main river), which coincides with the downstream most gauging station for most river systems (e.g., United States Geological Survey gauging stations and HyBAm database for South American rivers). More importantly, although the graph model contains simple Type II nodal relations, the predictions of water discharge, and total and suspended sediment discharge, are in similar agreement with field measurement as Type I models (Figures 6e–6g). As a result, the graph model developed herein is suitable for large spatial scale modeling applications, whereby existing field data are limited and collection costly. This is also supported by good agreements between uncalibrated graph model prediction and field measured water discharge for both Lena River and Wax Lake deltas (Figure 9).

Bedload discharge in the Selenga Delta is poorly predicted by the graph model. Since the Type II nodal relation of bedload discharge performs well, such discrepancy is perhaps due to inaccurate bedload discharge measurements at the Selenga River delta apex (Figure 3h). Therefore, future testing is necessary to better assess the graph model predictions of time series bedload discharge measurements. Moreover, cumulative

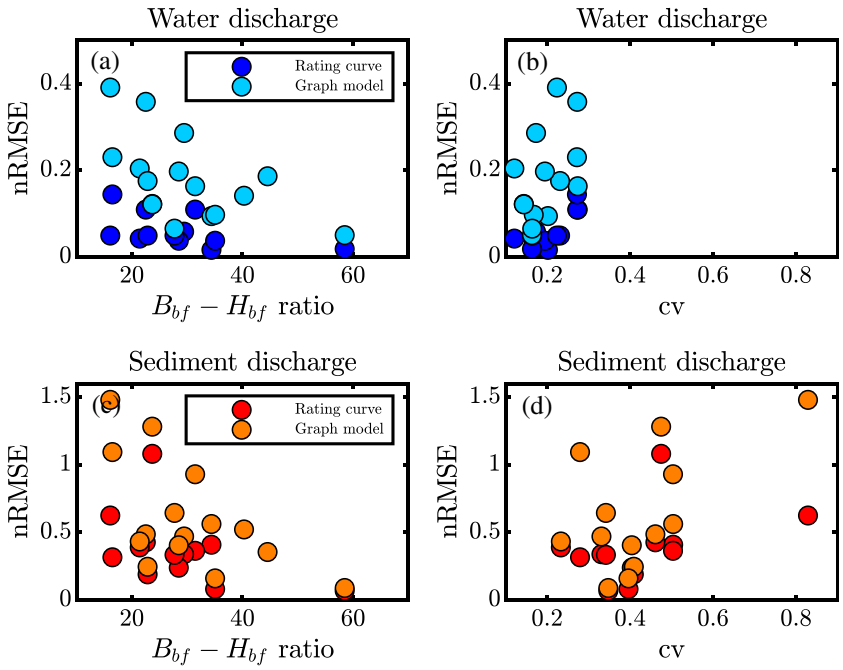

Figure 10. Normalized root-mean-square error as a function of bankfull width and depth ratio for rating curve and graph model predicted (a) water and (c) sediment discharge. Normalized root-mean-square error as a function of coefficient of variation for rating curve and graph model predicted (a) water and (c) sediment discharge.

bedload flux, on average, accounts for 3.9% of the cumulative suspended sediment flux (full range 0.013–12.8%) for the Selenga River delta, calculated using field measurements collected during the first month of field survey (see details in the supporting information). Similarly, instantaneous bedload flux, on average, accounts for 4.4% of the instantaneous suspended sediment flux (full range 0.0014–41.6%) for the Selenga River delta. The findings herein are consistent with other sand-bed river systems, whereby cumulative bedload sediment flux is 5% of cumulative suspended sediment flux (Nittrouer et al., 2008), and the instantaneous ratios of the two fluxes range from 1–75% (Ashley et al., 2020). Since bedload discharge does not account for a large proportion of the overall sediment volume, poor predictions based on the graph model do not significantly affect the overall sediment flux estimate.

One model limitation is the poor constraint on flow partitioning in regions of unconfined flow, as shown by a weaker model predictability for the Wax Lake delta (i.e., explaining 8% less variance in measured values than the predictions for Lena River delta; Figure 9c). One potential reason for such a lack of performance is that a significant portion of the flow in the Wax Lake delta is unconfined: ~59% leaves the channel and enters into adjacent wetlands, island interiors, and interdistributary bays, rather than flowing downstream to the tips of the distributary channels (Hiatt & Passalacqua, 2015; Shaw et al., 2016). In contrast, field measurements of water discharge in the Lena River delta were collected in regions of confined flow, which generated strong agreement with predictions.

An additional limitation of this framework is the lack of morphodynamic feedback. As flow varies, sediment transport and hydraulic conditions covary, and the channel network will undergo changes including avulsions and channel migration, which in turn will modify the channel network. There is no treatment of morphodynamic adjustments in the current framework, other than remapping a new channel network. Moreover, changes in channel morphology can also impact the stability regimes of individual bifurcations, leading to changes in flow partitioning locally. Bifurcation stability is presently not considered by the graph model but remains an important future task to address.

Presently, flow partitioning is assumed to be steady in the graph model. This is a reasonable assumption, because for the Selenga River delta, the difference in flux distribution between low and flood conditions is small (Figure 5), especially for channels that convey a larger proportion of the main river discharge (i.e.,

$F > 10\%$). However, predictability of both graph and rating curve models decreases with decreasing channel dimension (as indicated by an increase in nRMSE; Figures 10a and 10c). This is because smaller channels experience greater discharge change as stage varies from low to flood conditions (up to double that of the low flow discharge), while larger channels show only ~1–3% difference in discharge between low and flood conditions (Figures 5c, 10b, and 10d). Such findings are intuitive: Larger channels convey a significant proportion of the main river flow, so that discharge variability relative to the main channel is small.

Flux distribution at the network scale is dictated by regional hydraulics. The western portion of the delta has the steepest channel gradient, as well as the largest average cross-sectional area and depth, which allows for greater accommodation of flow (Table 3; Dong et al., 2016, 2019). Because bedload transport has a stronger dependency on flow depth (i.e., linked to shear stress) compared to suspended sediment flux, the western portion of the delta conveys a larger proportion of bedload flux (Figure 4d). In contrast, the middle portion of the delta has the smallest flow area (Table 3). Despite the aforementioned limitations, the graph model developed herein provides an effective tool for predicting flux distribution in delta networks in the absence of field data.

6. Conclusions

In this study, discharge data covering low to flood conditions, measured during a 6-week-long field survey of the Selenga River delta, are used to evaluate nodal relations of different variables to assess flow partitioning. These nodal relations are categorized and parsed as Type I (field measured) and Type II (remotely sensed) based on data collection methods for the variables, to explore model applicability for large delta systems, where data and field accessibility are limited. For Type I relations, cross-sectional area and flow depth are the best parameters for predicting water discharge partitioning, and water discharge is the best parameter for predicting total, suspended, and bedload sediment discharge partitioning. For Type II relations, a combination of width and sinuosity is the best parameter for predicting total and suspended sediment, and water discharge partitioning, and a combination of width and bifurcation angle is the best parameter for predicting bedload discharge partitioning. The best predictive Type II relations are incorporated into a graph model to generate a generalized framework to predict flux distribution in delta networks based solely on remotely sensed variables. Graph model predicted total and suspended sediment, and water discharge, are in agreement with field measurements. However, bedload discharge is poorly predicted by the graph model, implying that direct field measurements are still the best option to obtain reliable data. The graph model is further tested by predicting flux distribution in the Wax Lake and Lena River deltas, whereby predictions are in agreement with field measurements. As a result, the graph model is a very useful tool to constrain flow partitioning in deltas, as these systems usually lack gauge data in their distributary networks.

Appendix A: Selection of Variables in the Nodal Relations

Flow and sediment transport at a bifurcation are evaluated to determine the set of variables to use in a nodal relation. Mass balance of water discharge at the bifurcation follows (Bolla Pittaluga et al., 2003)

$$Q_a = Q_b + Q_c, \tag{A1}$$

where Q is water discharge, subscripts a–c denote the upstream and downstream branches, and water surface elevation (h) for three branches at the bifurcation node is assumed to be equivalent. Assuming steady and uniform flow, Q is expressed as (Garcia, 2008)

$$Q_i = C_{z,\,i}\sqrt{gH_iS_i}A_i, \tag{A2}$$

where g is gravitational acceleration, H is depth, A is cross-sectional area, S is bed slope, C_z is the dimensionless Chezy coefficient, and i is an index for branches a–c.

Similarly, mass balance of sediment discharge at the bifurcation follows (Bolla Pittaluga et al., 2003)

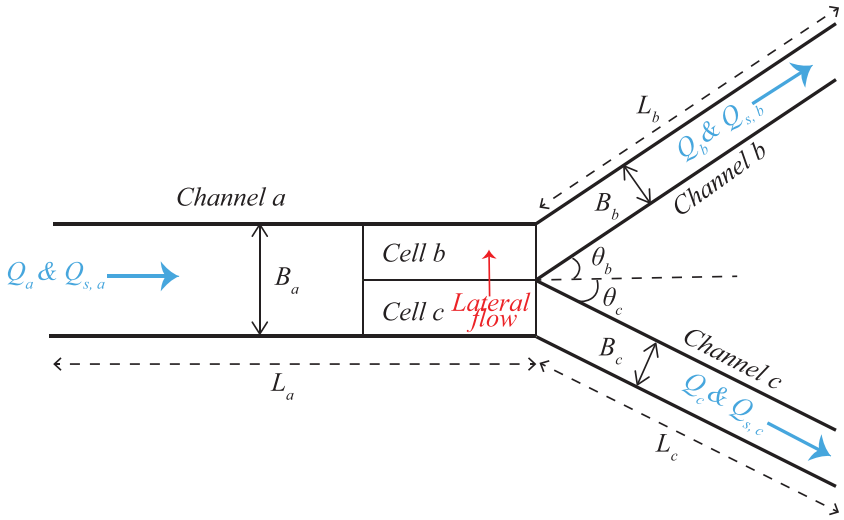

Figure A1. Schematic of a bifurcation and notations (see Table 1 for details) from a 1-D model (after Bolla Pittaluga et al., 2003). Blue arrows indicate the directions of water and sediment flow. Red arrow indicates the direction of lateral water and sediment flow between two cells upstream of the bifurcation.

$$Q_{s,a} = Q_{s,b} + Q_{s,c}, \tag{A3}$$

where Q_s is the total sediment load and expressed as the following for sand-bed channels (Engelund & Hansen, 1967):

$$Q_{s,i} = \sqrt{RgD_i^3} C_{z,i}^2 \tau_{*,i}^{2.5} B_i, \tag{A4}$$

where R is the submerged specific gravity, D is bed sediment size, and B is width, τ_* is the Shields number, equals to $\tau_* = HS/RD$ under normal flow condition, which is combined with the above total load relation and yield (Equation A4):

$$Q_{s,i} = \frac{g^{0.5} C_{z,i}^2 H_i^{2.5} S_i^{2.5} B_i}{R^2 D_i} \tag{A5}$$

Hydraulic variables in the mass and momentum balance and sediment transport equations necessitate field constraints, except for channel width (Equations A1–A4). Since slope controls the fluid stress along a channel reach, it is modified to incorporate more remotely sensible planform variables into the nodal relations. Specifically, assuming the receiving basin level (h_{basin}) is the same for both downstream branches, reach-averaged slope is related to planform variables (e.g., channel length and sinuosity) as (Salter et al., 2018)

$$S_i = \frac{h_i - h_{basin}}{\Omega_i L_{s,i}}, \tag{A6}$$

where h_i is the water surface elevation at the bifurcation, Ω is sinuosity, and L_s is the Euclidean distance between bifurcation nodes.

Based on the aforementioned assumptions on upstream and downstream water surface elevations, the ratio of reach average water surface slope is simplified to the ratio of channel length between the two downstream branches, and expressed as $\sqrt{S_b/S_c} = \sqrt{(1/L_b)/(1/L_c)} = \sqrt{L_c/L_b}$ (Equation A2). Furthermore, because sinuosity is related to channel length, the following relation between water discharge, slope, sinuosity, and length is obtained:

$$\frac{Q_b}{Q_c} \sim \sqrt{\frac{S_b}{S_c}} = \sqrt{\frac{\Omega_c L_{s,c}}{\Omega_b L_{s,b}}}. \tag{A7}$$

Similarly, sediment partitioning is also related to channel slope, sinuosity, and length as follows:

$$\frac{Q_{s,b}}{Q_{s,c}} \sim \left(\frac{S_b}{S_c}\right)^{2.5} = \left(\frac{\Omega_c L_{s,c}}{\Omega_b L_{s,b}}\right)^{2.5} \tag{A8}$$

The above relations indicate that a channel with higher sinuosity conveys a smaller proportion of flow, which is consistent with previous findings that a river channel with a higher sinuosity tends to have a greater form drag (Garcia, 2008; Garcia & Niño, 1993; Nelson & Smith, 1989).

Additional channel planform variables that are closely related to in-channel flow and sediment transport, include radius of curvature (R_c), nourishment area (A_n), and bifurcation angle (Θ). R_c is closely associated with channel length and sinuosity as it is calculated as a function of streamwise distance and impacts the strength of secondary flow (Asahi et al., 2013; Fagherazzi et al., 2004; Sylvester et al., 2019; Van Dijk et al., 2014). Nourishment area (A_n) is a metric developed specifically for a distributary system that is analogous to drainage area in tributary channels. It is defined by tracing the largest downstream area that a given channel bifurcation node could nourish (Edmonds et al., 2011). Nourishment area and channel length are found to follow Hack's law scaling relation, implying that distributary systems self-organize to maximize diversity of the outflow (i.e., optimality; Edmonds et al., 2011; Tejedor et al., 2017). Furthermore, increasing bifurcation angle (Θ) is found to reduce the volume of sediment deposition in the downstream branches (Szewczyk et al., 2020). A complete list of evaluated variables is shown in Table 1 and chosen as they are the hydraulic and planform parameters that control in-channel flow and sediment transport. In the nodal relations, these variables do not retain the power of their theoretical forms to avoid biases, such that depth is expressed as H for predicting water and sediment partitioning, respectively (Table 1 and Equations A2 and A4).

Appendix B: AIC

To compare the relative predictive quality between various nodal relations, the AIC is used (Akaike, 1974). For linear problems, AIC is expressed as the following (Banks & Joyner, 2017):

$$AIC = n \ln\left(\frac{RSS}{n}\right) + 2K. \tag{B1}$$

Here n is the number of observations, RSS is the residual sum of the squares, equal to $\sum_{i=1}^{n}(y_i - \hat{y}_i)^2$, y is the observed value (i.e., field measured flow partitioning), $\hat{y}$ is the predicted value by the nodal relations, and K is the number of independent variables (i.e., x_b and x_c from the main text). Note that the AIC method does not test the null hypothesis; instead, it provides a measurement of how close predicted distributions are from different models to the true distribution for a given set of data. More details of the AIC method can be found in Anderson and Burnham (2004).

Appendix C: Cross Correlation of Hydrographs

Cross correlation between hydrographs measured at the main river and at each transect is conducted using the signal processing tool box in MATLAB (i.e., xcorr, Figure C1). Water discharge is standardized via $z_Q = (Q - \overline{Q})/\sigma_Q$, where $\overline{Q}$ and σ_Q are mean and standard deviation of the water discharge, respectively. In summary, there are no significant lags between the hydrographs, by which implies that flood peaks arrive near synchronously everywhere in the Selenga River delta (Figure C1).

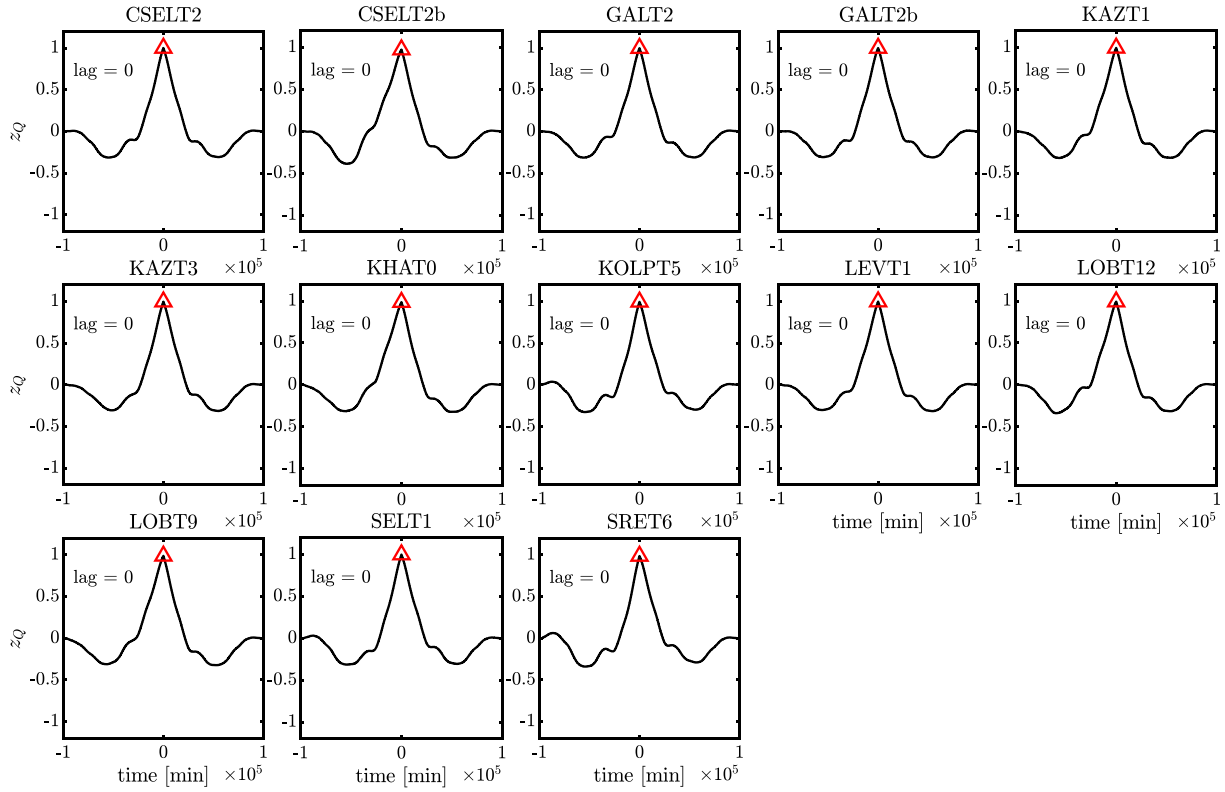

Figure C1. Cross correlation between hydrographs measured at the main river and at each transect.

Notation

A	Cross-sectional area
A_n	Nourishment area
B	Width
C_z	Dimensionless Chezy coefficient
F	Normalized flux, ratio of water discharge at individual branch to main river
H	Thalweg depth
L	Branch length
Q_a	Water discharge in the upstream branch
Q_b	Water discharge in one downstream branch
Q_c	Water discharge in the other downstream branch
Q_i	Water discharge in a branch
Q_{main}	Water discharge in the main river
$Q_{s,a}$	Sediment discharge in the upstream branch
$Q_{s,b}$	Sediment discharge in one downstream branch
$Q_{s,c}$	Sediment discharge in the other downstream branch
R_c	Radius of curvature
S	Water surface slope
Ω	Sinuosity
Θ	Bifurcation angle

Data Availability Statement

Hydraulic data generated during this study are displayed in the supporting information files and available for download at this OSF data repository (https://osf.io/2y4dq/).

Acknowledgments

This research is supported by funding from AAPG Foundation Grants-in-Aid, GSA Graduate Student Research Grant, University of Wyoming, Rice University, and in part by National Science Foundation grant EAR-1415944. E. Il'icheva and M. Pavlov are supported by RFBR grant No. 17-29-05052. V. Moreido is supported by the RFBR grant No. 17-29-05027. A. J. Moodie was supported by a NSF Graduate Research Fellowship under Grant No. 1842494. The research work on which this manuscript is based was carried out in cooperation with the international research initiative Basenet (Baikal-Selenga Network). We would like to thank Maarten van der Vegt and two anonymous reviewers for providing insightful comments and edits that significantly improved the quality of this manuscript. We thank students and staff from Irkutsk State, Saint Petersburg State, and Lomonosov Moscow State University for their assistance during the field survey. The authors would also like to thank the staff at V.B. Sochava Institute of Geography for processing the sediment samples and for providing assistance in the field. We thank Eric Barefoot for the useful discussion on model selection methods.

References

Akaike, H. (1974). A new look at the statistical model identification. *IEEE Transactions on Automatic Control*, *19*(6), 716–723.

Anderson, D., & Burnham, K. (2004). *Model selection and multi-model inference* (2nd ed., Vol. 63). NY: Springer-Verlag.

Asahi, K., Shimizu, Y., Nelson, J., & Parker, G. (2013). Numerical simulation of river meandering with self-evolving banks. *Journal of Geophysical Research: Earth Surface*, *118*, 2208–2229. https://doi.org/10.1002/jgrf.20150

Ashley, T. C., McElroy, B., Buscombe, D., Grams, P. E., & Kaplinski, M. (2020). Estimating bedload from suspended load and water discharge in sand bed rivers. *Water Resources Research*, *56*, e2019WR025883. https://doi.org/10.1029/2019WR025883

Banks, H. T., & Joyner, M. L. (2017). Aic under the framework of least squares estimation. *Applied Mathematics Letters*, *74*, 33–45.

Bertoldi, W., & Tubino, M. (2007). River bifurcations: Experimental observations on equilibrium configurations. *Water Resources Research*, *43*, W10437. https://doi.org/10.1029/2007WR005907

Blum, M. D., & Roberts, H. H. (2009). Drowning of the Mississippi Delta due to insufficient sediment supply and global sea-level rise. *Nature Geoscience*, *2*(7), 488.

Bolla Pittaluga, M., Coco, G., & Kleinhans, M. G. (2015). A unified framework for stability of channel bifurcations in gravel and sand fluvial systems. *Geophysical Research Letters*, *42*, 7521–7536. https://doi.org/10.1002/2015GL065175

Bolla Pittaluga, M., Repetto, R., & Tubino, M. (2003). Channel bifurcation in braided rivers: Equilibrium configurations and stability. *Water Resources Research*, *39*(3), 1046. https://doi.org/10.1029/2001WR001112

Chalov, S., Thorslund, J., Kasimov, N., Aybullatov, D., Il'icheva, E., Karthe, D., et al. (2016). The Selenga River delta: A geochemical barrier protecting Lake Baikal waters. *Regional Environmental Change*, *17*, 2039–2053.

Coffey, T. S., & Shaw, J. B. (2017). Congruent bifurcation angles in river delta and tributary channel networks. *Geophysical Research Letters*, *44*, 11,427–11,436. https://doi.org/10.1002/2017GL074873

Dong, T. Y., Nittrouer, J. A., Czapiga, M. J., Ma, H., McElroy, B., Il'icheva, E., et al. (2019). Roles of bank material in setting bankfull hydraulic geometry as informed by the Selenga River delta, Russia. *Water Resources Research*, *55*, 827–846. https://doi.org/10.1029/2017WR021985

Dong, T. Y., Nittrouer, J. A., Il'icheva, E., Pavlov, M., McElroy, B., Czapiga, M. J., et al. (2016). Controls on gravel termination in seven distributary channels of the Selenga River delta, Baikal Rift basin, Russia. *Geological Society of America Bulletin*, *128*(7–8), 1297–1312.

Dunne, K. ieranB. J., & Jerolmack, D. J. (2020). What sets river width? *Science Advances*, *6*(41), eabc1505.

Edmonds, D. A. (2009). The growth and evolution of river-dominated deltas and their distributary networks.

Edmonds, D. A., Paola, C., Hoyal, D. C. J. D., & Sheets, B. A. (2011). Quantitative metrics that describe river deltas and their channel networks. *Journal of Geophysical Research*, *116*, F04022. https://doi.org/10.1029/2010JF001955

Edmonds, D. A., & Slingerland, R. L. (2008). Stability of delta distributary networks and their bifurcations. *Water Resources Research*, *44*, W09426. https://doi.org/10.1029/2008WR006992

Emmett, W. W. (1979). *A field calibration of the sediment-trapping characteristics of the Helley-Smith bedload sampler* (Vol. 1139). US Government Printing Office.

Engelund, F., & Hansen, E. (1967). A monograph on sediment transport in alluvial streams. *Technical University of Denmark 0stervoldgade 10*. Copenhagen K.

Fagherazzi, S., Gabet, E. J., & Furbish, D. J. (2004). The effect of bidirectional flow on tidal channel planforms. *Earth Surface Processes and Landforms: The Journal of the British Geomorphological Research Group*, *29*(3), 295–309.

Fedorova, I., Chetverova, A., Bolshiyanov, D., Makarov, A., Boike, J., Heim, B., et al. (2015). Lena delta hydrology and geochemistry: Long-term hydrological data and recent field observations. *Biogeosciences*, *12*(2), 345–363.

Garcia, M. (2008). Sedimentation engineering: Processes, measurements, modeling, and practice. American Society of Civil Engineers.

Garcia, M., & Niño, Y. (1993). Dynamics of sediment bars in straight and meandering channels: Experiments on the resonance phenomenon. *Journal of Hydraulic Research*, *31*(6), 739–761.

Gleason, C. J., & Smith, L. C. (2014). Toward global mapping of river discharge using satellite images and at-many-stations hydraulic geometry. *Proceedings of the National Academy of Sciences*, *111*(13), 4788–4791.

Graf, W. L. (2006). Downstream hydrologic and geomorphic effects of large dams on American rivers. *Geomorphology*, *79*(3), 336–360.

Gyninova, A. B., & Korsunov, V. M. (2006). The soil cover of the Selenga Delta area in the Baikal region. *Eurasian Soil Science*, *39*(3), 243–250.

Hack, J. T. (1957). Studies of longitudinal stream profiles in Virginia and Maryland. (Vol. 294), US Government Printing Office.

Heiri, O., Lotter, A. F., & Lemcke, G. (2001). Loss on ignition as a method for estimating organic and carbonate content in sediments: Reproducibility and comparability of results. *Journal of Paleolimnology*, *25*(1), 101–110.

Hiatt, M. R. (2013). A network-based analysis of river delta surface hydrology: An example from wax lake delta.

Hiatt, M. R., & Passalacqua, P. (2015). Hydrological connectivity in river deltas: The first-order importance of channel-island exchange. *Water Resources Research*, *51*, 2264–2282. https://doi.org/10.1002/2014WR016149

Hiatt, M. R., & Passalacqua, P. (2017). What controls the transition from confined to unconfined flow? analysis of hydraulics in a coastal river delta (Ph.D. Thesis). American Society of Civil Engineers.

Hiatt, M. R., Sonke, W., Addink, E., van Dijk, W., van Kreveld, M., Ophelders, T., et al. (2019). Geometry and topology of estuary and braided river channel networks automatically extracted from topographic data.

Hoitink, A. J. F., Nittrouer, J. A., Passalacqua, P., Shaw, J. B., Langendoen, E. J., Huismans, Y., & van Maren, D. S. (2020). Resilience of river deltas in the Anthropocene. *Journal of Geophysical Research: Earth Surface*, *125*, e2019JF005201. https://doi.org/10.1029/2019JF005201

Il'icheva, E. A. (2008). Dynamics of the Selenga River network and delta structure. *Geography and Natural Resources*, *29*(4), 343–347.

Il'icheva, E. A., Gagarinova, O. V., & Pavlov, M. V. (2015). Hydrologo-geomorphological analysis of landscape formation within the Selenga River delta. *Geography and Natural Resources*, *36*(3), 263–270.

Isikdogan, F., Bovik, A., & Passalacqua, P. (2017a). RivaMap: An automated river analysis and mapping engine. *Remote Sensing of Environment*, *202*, 88–97.

Isikdogan, F., Bovik, A. C., & Passalacqua, P. (2017b). Surface water mapping by deep learning. *IEEE Journal of Selected Topics in Applied Earth Observations and Remote Sensing*, *10*(11), 4909–4918.

Kleinhans, M. G., Cohen, K. M., Hoekstra, J., & IJmker, J. M. (2011). Evolution of a bifurcation in a meandering river with adjustable channel widths, Rhine delta apex, The Netherlands. *Earth Surface Processes and Landforms*, *36*(15), 2011–2027.

Kleinhans, M. G., Jagers, H. R. A., Mosselman, E., & Sloff, C. J. (2008). Bifurcation dynamics and avulsion duration in meandering rivers by one-dimensional and three-dimensional models. *Water Resources Research*, *44*, W08454. https://doi.org/10.1029/2007WR005912

Krivonogov, S. K., & Safonova, I. Y. (2017). Basin structures and sediment accumulation in the baikal rift zone: Implications for Cenozoic intracontinental processes in the central Asian orogenic belt. *Gondwana Research*, *47*, 267–290.

Leopold, L. B., & Maddock, T. (1953). *The hydraulic geometry of stream channels and some physiographic implications* (Vol. 252). US Government Printing Office.

Liang, M., Geleynse, N., Edmonds, D. A., & Passalacqua, P. (2015). A reduced-complexity model for river delta formation—Part 2: Assessment of the flow routing scheme. *Earth Surface Dynamics*, *3*(1), 87.

Magritsky, D. V., Alexeevsky, N., Aybulatov, D., Fofonova, V., & Gorelkin, A. (2018). Features and evaluations of spatial and temporal changes of water runoff, sediment yield and heat flux in the Lena River delta. *Polarforschung*, *87*(2), 89–110.

Miori, S., Repetto, R., & Tubino, M. (2006). A one-dimensional model of bifurcations in gravel bed channels with erodible banks. *Water Resources Research*, *42*, W11413. https://doi.org/10.1029/2006WR004863

Nelson, J. M., & Smith, J. D. (1989). Flow in meandering channels with natural topography. *River Meandering*, *12*, 69–102.

Nienhuis, J. H., Ashton, A. D., Edmonds, D. A., Hoitink, A. J. F., Kettner, A. J., Rowland, J. C., & Törnqvist, T. E. (2020). Global-scale human impact on delta morphology has led to net land area gain. *Nature*, *577*(7791), 514–518.

Nittrouer, J. A., Allison, M. A., & Campanella, R. (2008). Bedform transport rates for the lowermost Mississippi River. *Journal of Geophysical Research*, *113*, F03004. https://doi.org/10.1029/2007JF000795

Paola, C., Twilley, R. R., Edmonds, D. A., Kim, W., Mohrig, D., Parker, G., et al. (2011). Natural processes in delta restoration: Application to the Mississippi Delta. *Annual Review of Marine Science*, *3*, 67–91.

Parker, G. (1978a). Self-formed straight rivers with equilibrium banks and mobile bed. Part 1. The sand-silt river. *Journal of Fluid Mechanics*, *89*(1), 109–125.

Parker, G. (1978b). Self-formed straight rivers with equilibrium banks and mobile bed. Part 2. The gravel river. *Journal of Fluid Mechanics*, *89*(1), 127–146.

Passalacqua, P. (2017). The Delta Connectome: A network-based framework for studying connectivity in river deltas. *Geomorphology*, *277*, 50–62.

Passalacqua, P., Lanzoni, S., Paola, C., & Rinaldo, A. (2013). Geomorphic signatures of deltaic processes and vegetation: The Ganges-Brahmaputra-Jamuna case study. *Journal of Geophysical Research: Earth Surface*, *118*, 1838–1849. https://doi.org/10.1002/jgrf.20128

Pavlov, M. V., Il'icheva, E. A., Vershinin, K. E., & Kobylkin, D. V. (2019). Development of the lakes of the Selenga River delta in the late Holocene (in Russian). *Bulletin of The Buryat State University*, *1*(3), 31–43.

Pietroń, J., Nittrouer, J. A., Chalov, S. R., Dong, T. Y., Kasimov, N., Shinkareva, G., & Jarsjö, J. (2018). Sedimentation patterns in the Selenga River delta under changing hydroclimatic conditions. *Hydrological processes*, *32*(2), 278–292.

Piliouras, A., & Rowland, J. (2019). Arctic delta Landsat image classifications.

Rantz, S. E., et al. (1982). Measurement and computation of streamflow: Volume 1, measurement of stage and discharge (Tech. Rep.). USGPO.

Redolfi, M., Zolezzi, G., & Tubino, M. (2019). Free and forced morphodynamics of river bifurcations. *Earth Surface Processes and Landforms*, *44*(4), 973–987.

Salter, G., Paola, C., & Voller, V. R. (2018). Control of delta avulsion by downstream sediment sinks. *Journal of Geophysical Research: Earth Surface*, *123*, 142–166. https://doi.org/10.1002/2017JF004350

Schielen, R. alphM. J., & Blom, A. (2018). A reduced complexity model of a gravel-sand river bifurcation: Equilibrium states and their stability. *Advances in Water Resources*, *121*, 9–21.

Schwenk, J., Piliouras, A., & Rowland, J. C. (2019). Determining flow directions in river channel networks using planform morphology and topology. *Earth Surface Dynamics Discussions*, *2019*, 1–23. https://doi.org/10.5194/esurf-2019-19

Shaw, J. B., Mohrig, D., & Wagner, R. W. (2016). Flow patterns and morphology of a prograding river delta. *Journal of Geophysical Research: Earth Surface*, *121*, 372–391. https://doi.org/10.1002/2015JF003570

Slingerland, R., & Smith, N. D. (1998). Necessary conditions for a meandering-river avulsion. *Geology*, *26*(5), 435–438.

Sylvester, Z., Durkin, P., & Covault, J. A. (2019). High curvatures drive river meandering. *Geology*, *47*(3), 263–266.

Syvitski, J. P. M., Kettner, A. J., Overeem, I., Hutton, E. W., Hannon, M. T., Brakenridge, G. R., et al. (2009). Sinking deltas due to human activities. *Nature Geoscience*, *2*(10), 681.

Syvitski, J. P. M., & Saito, Y. (2007). Morphodynamics of deltas under the influence of humans. *Global and Planetary Change*, *57*(3), 261–282.

Syvitski, J. P. M., Vörösmarty, C. J., Kettner, A. J., & Green, P. (2005). Impact of humans on the flux of terrestrial sediment to the global coastal ocean. *Science*, *308*(5720), 376–380.

Szewczyk, L., Grimaud, J.-L., & Cojan, I. (2020). Experimental evidences for bifurcation angles control on abandoned channel fill geometry. *Earth Surface Dynamics Discussions*, *2020*, 1–23. https://doi.org/10.5194/esurf-2019-79

Szupiany, R. N., Amsler, M. L., Hernandez, J., Parsons, D. R., Best, J. L., Fornari, E., & Trento, A. (2012). Flow fields, bed shear stresses, and suspended bed sediment dynamics in bifurcations of a large river. *Water Resources Research*, *48*, W11515. https://doi.org/10.1029/2011WR011677

Tejedor, A., Longjas, A., Edmonds, D. A., Zaliapin, I., Georgiou, T. T., Rinaldo, A., & Foufoula-Georgiou, E. (2017). Entropy and optimality in river deltas. *Proceedings of the National Academy of Sciences*, *114*(44), 11,651–11,656.

Tejedor, A., Longjas, A., Passalacqua, P., Moreno, Y., & Foufoula-Georgiou, E. (2018). Multiplex networks: A framework for studying multiprocess multiscale connectivity via coupled-network theory with an application to river deltas. *Geophysical Research Letters*, *45*, 9681–9689. https://doi.org/10.1029/2018GL078355

Tejedor, A., Longjas, A., Zaliapin, I., & Foufoula-Georgiou, E. (2015a). Delta channel networks: 1. A graph-theoretic approach for studying connectivity and steady state transport on deltaic surfaces. *Water Resources Research*, *51*, 3998–4018. https://doi.org/10.1002/2014WR016577

Tejedor, A., Longjas, A., Zaliapin, I., & Foufoula-Georgiou, E. (2015b). Delta channel networks: 2. Metrics of topologic and dynamic complexity for delta comparison, physical inference, and vulnerability assessment. *Water Resources Research*, *51*, 4019–4045. https://doi.org/10.1002/2014WR016604

Van, C. P., Gourgue, O., Sassi, M., Hoitink, A. J. F., Deleersnijder, E., & Soares-Frazão, S. (2016). Modelling fine-grained sediment transport in the Mahakam land-sea continuum, Indonesia. *Journal of Hydro-Environment Research*, *13*, 103–120.

Van Dijk, W. M., Schuurman, F., Van de Lageweg, W. I., & Kleinhans, M. G. (2014). Bifurcation instability and chute cutoff development in meandering gravel-bed rivers. *Geomorphology*, *213*, 277–291.

Vörösmarty, C. J., Syvitski, J., Day, J., de Sherbinin, A., Giosan, L., & Paola, C. (2009). Battling to save the world's river deltas. *Bulletin of the Atomic Scientists*, *65*(2), 31–43.

Wang, Z. B., De Vries, M., Fokkink, R. J., & Langerak, A. (1995). Stability of river bifurcations in ID morphodynamic models. *Journal of Hydraulic Research*, *33*(6), 739–750.